catalysts

MDPI

Article

Adjusting *Ortho*-Cycloalkyl Ring Size in a Cycloheptyl-Fused *N,N,N*-Iron Catalyst as Means to Control Catalytic Activity and Polyethylene Properties

Mingyang Han [1,2], Qiuyue Zhang [1,2], Ivan I. Oleynik [3,*], Hongyi Suo [1,2], Irina V. Oleynik [3], Gregory A. Solan [1,4,*], Yanping Ma [1], Tongling Liang [1] and Wen-Hua Sun [1,2,5,*]

1 Key Laboratory of Engineering Plastics and Beijing National Laboratory for Molecular Sciences, Institute of Chemistry, Chinese Academy of Sciences, Beijing 100190, China; hanmingyang@iccas.ac.cn (M.H.); zhangqiuyue@iccas.ac.cn (Q.Z.); suohongyi@iccas.ac.cn (H.S.); myanping@iccas.ac.cn (Y.M.); ltl@iccas.ac.cn (T.L.)
2 CAS Research/Education Center for Excellence in Molecular Sciences and International School, University of Chinese Academy of Sciences, Beijing 100049, China
3 N.N. Vorozhtsov Novosibirsk Institute of Organic Chemistry, Pr. Lavrentjeva 9, Novosibirsk 630090, Russia; olk@nioch.nsc.ru
4 Department of Chemistry, University of Leicester, University Road, Leicester LE1 7RH, UK
5 State Key Laboratory for Oxo Synthesis and Selective Oxidation, Lanzhou Institute of Chemical Physics, Chinese Academy of Sciences, Lanzhou 730000, China
* Correspondence: oleynik@nioch.nsc.ru (I.I.O.); gas8@leicester.ac.uk (G.A.S.); whsun@iccas.ac.cn (W.-H.S.); Tel.: +7-383-330-9524 (I.I.O.); +44-116-252-2096 (G.A.S.); +86-10-6255-7955 (W.-H.S.)

Received: 8 August 2020; Accepted: 1 September 2020; Published: 2 September 2020

Abstract: Five examples of bis(arylimino)tetrahydrocyclohepta[*b*]pyridine dichloroiron(II) complex, [2-{(Ar)N=CMe}-9-{N(Ar)}$C_{10}H_{10}$N]$FeCl_2$ (Ar = 2-(C_5H_9)-4,6-$(CHPh_2)_2C_6H_2$ **Fe1**, 2-(C_6H_{11})-4,6-$(CHPh_2)_2C_6H_2$ **Fe2**, 2-(C_8H_{15})-4,6-$(CHPh_2)_2C_6H_2$ **Fe3**, 2-($C_{12}H_{23}$)-4,6-$(CHPh_2)_2C_6H_2$ **Fe4**, and 2,6-(C_5H_9)2-4-$(CHPh_2)C_6H_2$ **Fe5**), incorporating *ortho*-pairings based on either benzhydryl/cycloalkyl (ring sizes ranging from 5 to 12) or cyclopentyl/cyclopentyl groups, have been prepared in reasonable yield by employing a simple one-pot template strategy. Each complex was characterized by FT-IR spectroscopy, elemental analysis, and for **Fe3** and **Fe5** by single crystal X-ray diffraction; *pseudo*-square pyramidal geometries are a feature of their coordination spheres. On treatment of **Fe1**–**Fe5** with modified methylaluminoxane (MMAO) or methylaluminoxane (MAO), a range in catalytic activities for ethylene polymerization were observed with benzhydryl/cyclopentyl-containing **Fe1**/MMAO achieving the maximum level of 15.3×10^6 g PE mol^{-1} (Fe) h^{-1} at an operating temperature of 70 °C. As a key trend, the activity was found to drop as the *ortho*-cycloalkyl ring size increased: $\mathbf{Fe1}_{C5H9/CHPh2}$~$\mathbf{Fe5}_{C5H9/C5H9}$ > $\mathbf{Fe2}_{C6H11/CHPh2}$ > $\mathbf{Fe3}_{C8H15/CHPh2}$ > $\mathbf{Fe4}_{C12H23/CHPh2}$. Furthermore, strictly linear polyethylenes (T_m > 126 °C) were formed with molecular weights again dependent on the *ortho*-cycloalkyl ring size (up to 55.6 kg mol^{-1} for **Fe1**/MAO); narrow dispersities were a characteristic of all the polymers (M_w/M_n range: 2.3–4.7), highlighting the well-controlled nature of these polymerizations.

Keywords: iron(II) precatalysts; fused bis(imino)pyridine; *ortho*-cycloalkyl; *ortho*-benzhydryl; ethylene polymerization; structure–activity correlation; structure–molecular weight correlation

1. Introduction

The transition metal-catalyzed polymerization of ethylene is one of the most important carbon–carbon bond-forming reactions and moreover, it is widely used in the chemical industry [1,2].

Late transition metal complexes, and in particular those based on iron and cobalt [3–8], have emerged as effective catalysts in ethylene polymerization [9–13]; others involving the first row *d*-block centers such as nickel [14,15], chromium [16,17], and vanadium [18] have also shown great potential. While catalytic activity represents a key attribute of the catalyst, there is nowadays a drive toward systems that can operate effectively at high temperature whilst still producing high molecular weight polyethylene with a narrow molecular weight distribution. In this regard, variations to the classic bis(imino)pyridine-iron(II) halide structure [9–13] (**A**, Scheme 1) in the form of modifications to the *ortho*-/*para*-substitution pattern (i.e., steric and electronic effects) or even more dramatic structural changes to the *N*,*N*,*N*-ligand core itself have seen improvements in the catalytic performance and molecular weight of the polyolefin.

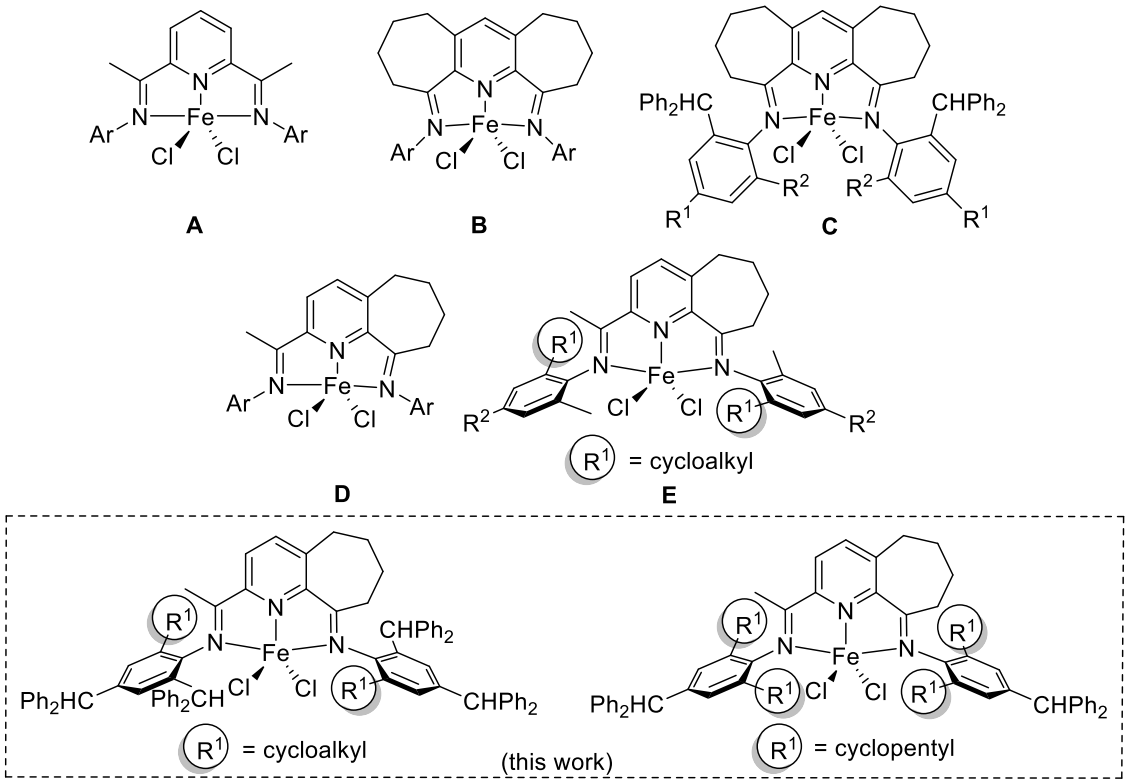

Scheme 1. From bis(imino)pyridine-iron precatalyst (**A**) to cycloheptyl-fused derivatives, (**B**–**E**).

Of note, iron catalysts bearing carbocyclic-fused bis(imino)pyridine ligands have shown a capacity to display optimal productivity at temperatures in the range of 50–80 °C. In particular, bis(imino)pyridines bearing doubly or singly fused seven-membered rings have provided robust ligand frameworks for a range of iron(II) precatalysts (**B**–**E**, Scheme 1) [19–24]. In terms of catalytic performance, doubly fused **B** [19] bearing relatively small *ortho*-alkyl substituents displayed excellent activity (up to 10^7 g PE mol^{-1} (Fe) h^{-1}) with the molecular weight of the resulting polyethylenes falling in the range of 3.5–96.9 kg mol^{-1} albeit with broad dispersity. By comparison, the installation of larger benzhydryl groups ($CHPh_2$) to the *ortho*-sites in **C** [20] led to similar high catalytic activities but afforded lower molecular weight polyethylene that exhibited narrower dispersity. For the singly fused iron(II) precatalysts **D** and **E** (Scheme 1), a noticeable increase in thermal stability was noted, especially for **E** in which the *ortho*-positions of the *N*-aryl group were substituted with cycloalkyl and hydrogen/methyl [22].

In this work, we revisit the singly-fused bis(arylimino)tetrahydrocyclohepta[*b*]pyridine skeleton shown in iron-containing **D** and **E**, with a view to introducing *N*-aryl *ortho*-pairings based on benzhydryl/cyclopentyl, benzhydryl/cyclohexyl, benzhydryl/cyclooctyl and benzhydryl/cyclododecyl; for comparative purposes, we also report the *ortho*-combination cyclopentyl/cyclopentyl (Scheme 1), as it is a common feature to all iron complexes to be synthesized is the presence of a *para*-benzhydryl group.

To explore the impact of the size of *ortho*-cycloalkyl ring on catalyst activity, thermal stability as well as various polymer properties, a comprehensive polymerization study is presented involving changes to the type/amount of co-catalyst, temperature, pressure, and run time. Additionally, the synthetic and characterization data for all new iron complexes are disclosed.

2. Results

2.1. Materials and Methods

The synthesis and handling of air- and moisture-sensitive compounds were carried out under an atmosphere of nitrogen using standard Schlenk techniques. Prior to use, toluene was heated under reflux over sodium/benzophenone and then distilled. Methylaluminoxane (MAO) (1.46 M solution in toluene) and modified methylaluminoxane (MMAO) (1.93 M solution in n-heptane) were purchased from Albemarle Corporation. High-purity ethylene was purchased from Beijing Yanshan Petrochemical Co. and used as received. Other reagents were purchased from Aldrich or local suppliers. IR spectra were recorded using a PerkinElmer System 2000 FT-IR spectrometer. Elemental analysis was carried out with a Flash EA 1112 microanalyzer. Molecular weights and molecular weight distributions of the polymers were determined with an Agilent PL 220 GPC instrument operating at 150 °C with 1,2,4-trichlorobenzene as solvent. Melting temperatures of the polyethylenes were measured from the second scanning run on a Perkin-Elmer DSC-7 differential scanning calorimeter (DSC) under a nitrogen atmosphere. ^{1}H and ^{13}C NMR spectra of the polyethylenes were recorded using a Bruker DMX 300 MHz instrument at 100 °C in deuterated 1,1,2,2-tetrachloroethane with tetramethylsilane (TMS) as an internal standard. The compounds 2-acetyl-5,6,7,8-tetrahydrocyclohepta[*b*]pyridin-9-one [25] and the 2-cycloalkylanilines [26–28] have been prepared using the literature methods.

*2.2. [2-{(Ar)N=CMe}-9-{N(Ar)}$C_{10}H_{10}N$]$FeCl_2$ (**Fe1**–**Fe5**)*

Ar = 2-(C_5H_9)-4,6-($CHPh_2$)$_2$$C_6H_2$ **Fe1**. A mixture of 2-acetyl-5,6,7,8-tetrahydrocyclohepta[*b*]pyridin -9-one (0.061 g, 0.30 mmol), 2-cyclopentyl-4,6-dibenzhydrylaniline (0.140 g, 0.66 mmol), and iron(II) chloride tetrahydrate (0.057 g, 0.29 mmol) in glacial acetic acid (20 mL) was stirred and heated under reflux for 3 h. Once cooled to ambient temperature, the solvent was partially removed under reduced pressure, and an excess of diethyl ether was added to induce precipitation. Then, the precipitate was collected, washed with diethyl ether (4 × 15 mL), and dried to afford **Fe1** as a green powder (0.197 g, 53%). FT-IR (cm^{-1}): 3025 (w), 2946 (m), 2865 (w), 1598 (m, ν(C=N)), 1569 (m), 1492 (s), 1448 (s), 1030 (m), 840 (w), 744 (m), 698 (s), 613 (m). Anal. Calcd for $C_{86}H_{79}Cl_2FeN_3$ (1281.34): C, 80.61; H, 6.21; N, 3.28. Found: C, 80.44; H, 6.16; N, 3.45%.

Ar = 2-(C_6H_{11})-4,6-($CHPh_2$)$_2$$C_6H_2$ **Fe2**. By employing the same procedure as that described for **Fe1** but with 2-cyclohexyl-4,6-dibenzhydrylaniline as the aniline, **Fe2** was isolated as a green powder (0.220 g, 58%). FT-IR (cm^{-1}): 3025 (w), 2927 (m), 1599 (m, ν(C=N)), 1572 (m), 1493 (s), 1447 (s), 1261 (m), 1030 (m), 744 (m), 698 (s), 614 (m). Anal. Calcd for $C_{88}H_{83}Cl_2FeN_3$ (1309.40): C, 80.72; H, 6.39; N, 3.21. Found: C, 80.48; H, 6.33; N, 3.44%.

Ar = 2-(C_8H_{15})-4,6-($CHPh_2$)$_2$$C_6H_2$ **Fe3**. By employing the same procedure as that described for **Fe1** but with 2-cyclooctyl-4,6-dibenzhydrylaniline as the aniline, **Fe3** was isolated as a green powder (0.246 g, 62%). FT-IR (cm^{-1}): 3025 (w), 2916 (m), 2854 (m), 1599 (m, ν(C=N)), 1572 (s), 1493 (s), 1446 (s), 1261 (m), 1030 (m), 744 (m), 697 (s), 613 (m). Anal. Calcd for $C_{92}H_{91}Cl_2FeN_3$ (1365.51): C, 80.92; H, 6.72; N, 3.08. Found: C, 80.71; H, 6.90; N, 3.12%.

Ar = 2-($C_{12}H_{23}$)-4,6-($CHPh_2$)$_2$$C_6H_2$ **Fe4**. By employing the same procedure as that described for **Fe1** but with 2-cyclododecyl-4,6-dibenzhydrylaniline as the aniline, **Fe4** was isolated as a green powder (0.171 g, 40%). FT-IR (cm^{-1}): 3025 (w), 2924 (m), 2856 (w), 1601 (m, ν(C=N)), 1571 (s), 1494 (s), 1030 (m), 744 (m), 699 (s), 614 (m). Anal. Calcd for $C_{100}H_{107}Cl_2FeN_3$ (1477.72): C, 81.28; H, 7.30; N, 2.84. Found: C, 81.38; H, 7.22; N, 3.04%.

Ar = 2,6-$(C_5H_9)_2$-4-$(CHPh_2)C_6H_2$ **Fe5**. By employing the same procedure as that described for **Fe1** but with 2,6-dicyclopentyl-4-benzhydrylaniline as the aniline, **Fe5** was isolated as a green powder (0.173 g, 55%). FT-IR (cm^{-1}): 3025 (w), 2948 (m), 2864 (m), 1598 (m, ν(C=N)), 1569 (s), 1491 (s), 1029 (m), 742 (m), 700 (s), 619 (m). Anal. Calcd for $C_{70}H_{75}Cl_2FeN_3$ (1085.14): C, 77.48; H, 6.97; N, 3.87. Found: C, 77.76; H, 6.80; N, 3.52%.

2.3. General Procedure for Ethylene Polymerization

A stainless steel autoclave (250 mL) containing an ethylene pressure control system, a mechanical stirrer, and a temperature controller was used to conduct the polymerization runs. The autoclave was placed under reduced pressure and backfilled with ethylene (×3). On reaching the required temperature, the iron complex (2 μmol), pre-dissolved in toluene (25 mL), was injected into the autoclave under an ethylene atmosphere (ca. 1 atm) followed by the addition of more toluene (25 mL). Subsequently, the specified quantity of co-catalyst (MMAO or MAO) was added by syringe, and finally, more was toluene introduced to bring the total volume of solvent to 100 mL. The apparatus was immediately pressurized to an ethylene pressure of 5 or 10 atm, and the stirring started. Following the set reaction time (5–60 min), the autoclave was allowed to cool to ambient temperature and the ethylene pressure was vented. The reaction mixture was quenched with 10% HCl in ethanol and the resulting polyethylene was filtered, washed with ethanol, and then finally dried at 60 °C until of constant weight.

2.4. X-ray Diffraction Studies

X-ray quality crystals of **Fe3** and **Fe5** were obtained by diffusing hexane onto a dichloromethane solution containing the corresponding complex. A single crystal of each was selected and mounted on a Bruker SMART CCD diffractometer incorporating a graphite-monochromated Mo–Kα radiation (λ = 0.71073 Å) source and a nitrogen cold stream (−100 °C). The data were corrected for Lorentz and polarization effects (SAINT) and semiempirical absorption corrections based on equivalent reflections were applied (SADABS). The structures were solved by direct methods and refined by full-matrix least-squares on F^2. Hydrogen atoms were placed in calculated positions. Structure solution and structure refinement were carried out by using the SHELXT (Sheldrick, 2018) [29]. The structural disorder exhibited by the cyclopentyl and dichloromethane solvent molecules in **Fe5** was also processed by the SHELXL (Sheldrick, 2018) [30]. The X-ray structure determination and refinement details are collected in Table 1.

Table 1. Crystallographic data and structure refinement for **Fe3** and **Fe5**.

-	Fe3	Fe5
Crystal color	blue	gray
Empirical formula	$C_{92}H_{91}Cl_2FeN_3$	$2\ C_{70}H_{75}Cl_2FeN_3{\cdot}3CH_2Cl_2$
Formula weight	1363.41	2424.93
T (K)	172(2)	173(2)
Wavelength (Å)	0.71073	0.71073
Crystal system	Tetragonal	Orthorhombic
Space group	$I4_1/a$	$P2_12_12_1$
a/Å	32.4190(2)	18.8805(6)
b/Å	32.4190(2)	19.1069(5)
c/Å	31.8280(3)	35.1775(10)
α/°	90	90
β/°	90	90
γ/°	90	90
Volume/$Å^3$	33,451.0(5)	12,690.2(6)
Z	16	4
$\rho_{calc}g/cm^3$	1.083	1.269
μ/mm^{-1}	2.359	0.492
F(000)	11,552.0	5112
Crystal size/mm^3	0.15 × 0.1 × 0.05	0.184 × 0.181 × 0.062

Table 1. *Cont.*

-	Fe3	Fe5
Θ range (°)	6.7 to 151.132	3.032 to 50
Limiting indices	−34 ≤ h ≤ 36 −35 ≤ k ≤ 40 −39 ≤ l ≤ 37	−22 ≤ h ≤ 22 −22 ≤ k ≤ 22 −41 ≤ l ≤ 39
No. of rflns collected	65,052	76,355
No. unique rflns [R(int)]	16,088(0.0368)	21,892(0.1219)
Completeness to θ (%)	96.2	99.8
Goodness of fit on F^2	1.024	1.024
Final R indices [I > 2σ(I)]	R_1 = 0.0531 wR_2 = 0.1370	R_1 = 0.0953 wR_2 = 0.2468
R indices (all data)	R_1 = 0.0623 wR_2 = 0.1425	R_1 = 0.1449 wR_2 = 0.2910
Largest diff peak and hole (e $Å^{-3}$)	0.99/−0.35	0.92/−0.56

3. Results and Discussion

3.1. Synthesis and Characterization of *Fe1–Fe5*

A one-pot strategy was utilized to synthesize the bis(arylimino)tetrahydrocyclohepta[*b*]pyridine dichloroiron(II) complexes, [2-{(Ar)N=CMe}-9-{N(Ar)}$C_{10}H_{10}$N]$FeCl_2$ (Ar = 2-(C_5H_9)-4,6-($CHPh_2$)$_2$ C_6H_2 **Fe1**, 2-(C_6H_{11})-4,6-($CHPh_2$)$_2C_6H_2$ **Fe2**, 2-(C_8H_{15})-4,6-($CHPh_2$)$_2C_6H_2$ **Fe3**, 2-($C_{12}H_{23}$)-4,6 -($CHPh_2$)$_2C_6H_2$ **Fe4**, and 2,6-(C_5H_9)$_2$-4-($CHPh_2$)C_6H_2 **Fe5**). Typically, by combining 2-acetyl-5,6,7,8-tetrahydrocyclohepta[*b*]pyridin-9-one, the respective aniline, and iron(II) chloride tetrahydrate in acetic acid under reflux for several hours, the target ferrous complexes could be isolated as green solids on work-up in reasonable yield (Scheme 2). All complexes have been characterized by FT-IR spectroscopy, elemental analysis, and for **Fe3** and **Fe5**, by X-ray diffraction.

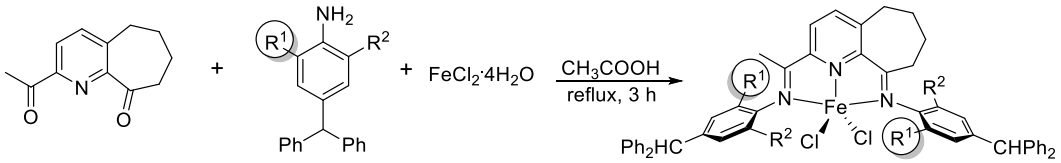

	Fe1	Fe2	Fe3	Fe4	Fe5
R^1	C_5H_9	C_6H_{11}	C_8H_{15}	$C_{12}H_{23}$	C_5H_9
R^2	$CHPh_2$	$CHPh_2$	$CHPh_2$	$CHPh_2$	C_5H_9
Yield (%)	53	58	62	40	55

Scheme 2. One-pot preparative route to **Fe1**–**Fe5**.

Single crystals of **Fe3** and **Fe5** of suitable quality for the X-ray determinations were obtained by diffusing hexane onto a dichloromethane solution containing the complex. X-ray crystallographic data for **Fe3** and **Fe5** can been found as Supplementary Materials from the Cambridge Crystallographic Data Centre (CCDC): 2021622 (**Fe3**), 2020110 (**Fe5**). Following the structure refinement of **Fe5**, two independent molecules (A and B) were evident within the asymmetric unit with only minimal differences apparent between them. Views of **Fe3** and **Fe5** (molecule A) are depicted in Figures 1 and 2; selected bond lengths and angles are tabulated in Table 2. The structures of **Fe3** and **Fe5** are similar differing only in the *N*-aryl group substitution pattern (*viz.* 2-cyclooctyl-4,6-dibenzhydrylphenyl **Fe3**, 2,6-dicyclopentyl-4-benzhydrylphenyl **Fe5**) and will be described together. Each structure contains an iron center coordinated to two chloride atoms and three nitrogen donors from the chelating *N*,*N*,*N*-ligand to form a geometry best identified as a distorted square pyramidal [17,19–24]. The square base of the pyramid is filled by the N1, N2, N3, and Cl2 while Cl1 occupies the apical position. The iron atom is located above the basal plane by 0.516 Å for **Fe3** and 0.623 Å for **Fe5**, which is

reminiscent of that seen in a number of structurally related analogs [22,23]. Of the three iron–nitrogen distances, the central Fe-$N_{pyridine}$ bond length [2.0826(17) Å for **Fe3** and 2.132(8) Å for **Fe5**] is the shortest, likely reflecting the constraints of the pincer ligand and the stronger donor ability of the pyridine nitrogen. The Fe-N_{imine} distances though longer are comparable despite their inequivalent environments [2.2256(18), 2.1972(17) Å (**Fe3**), 2.287(8), 2.292(8) Å (**Fe5**)]. The planes of the *N*-aryl groups are positioned almost perpendicularly to their adjacent imine vectors as is evidenced by the dihedral angles (71.1°, 82.5° **Fe3**; 82.2°, 86.5° **Fe5**), the first angle in each pair being slightly less on account of steric hindrance imposed by the neighboring pyridine-fused carbocyclic ring. As expected, the saturated section of the fused carbocycle (C7–C8–C9–C10) shows some deviation from planarity, owing to the sp^3-hybridization of these four carbon atoms. The *ortho*-substituted cycloalkyl groups display boat-chair/tub (**Fe3**$_{cyclooctyl}$) and envelope (**Fe5**$_{cyclopentyl}$) configurations.

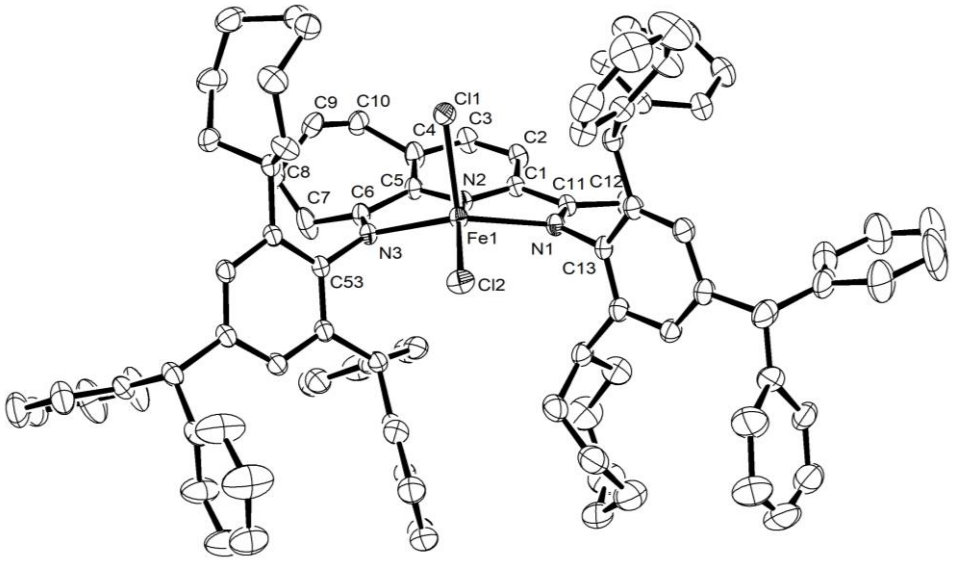

Figure 1. Molecular structure of **Fe3**. The thermal ellipsoids were set at the 30% probability level, while the hydrogen atoms have been removed for clarity.

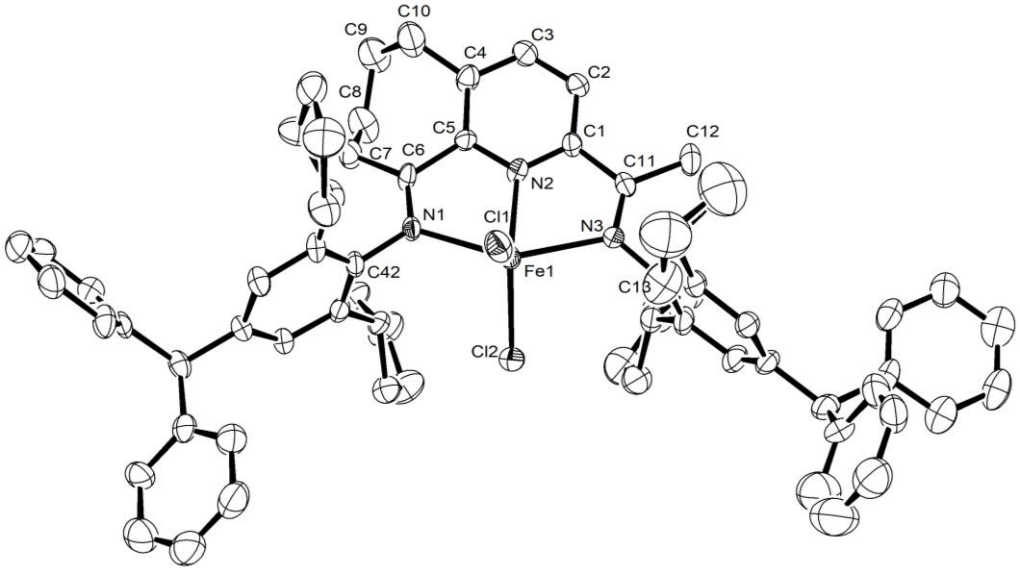

Figure 2. Molecular structure of **Fe5** (molecule A). The thermal ellipsoids were set at the 30% probability level, while the hydrogen atoms, molecule B, and three molecules of CH_2Cl_2 have been removed for clarity.

Table 2. Selected bond lengths and angles for **Fe3** and **Fe5** (molecule A).

-	Fe3	Fe5
-	Bond lengths (Å)	-
Fe(1)-N(1)	2.2256(18)	2.287(8)
Fe(1)-N(2)	2.0826(17)	2.132(8)
Fe(1)-N(3)	2.1972(17)	2.292(8)
Fe(1)-Cl(1)	2.3250(6)	2.316(4)
Fe(1)-Cl(2)	2.2456(6)	2.282(4)
-	Bond Angles (deg)	-
N(1)-Fe(1)-N(2)	73.48(6)	73.5(3)
N(1)-Fe(1)-N(3)	141.04(6)	144.8(3)
N(2)-Fe(1)-N(3)	73.23(6)	72.1(3)
N(1)-Fe(1)-Cl(2)	97.70(5)	102.0(2)
N(2)-Fe(1)-Cl(2)	152.55(6)	135.5(3)
N(3)-Fe(1)-Cl(2)	102.58(5)	97.2(2)
N(1)-Fe(1)-Cl(1)	104.23(5)	97.0(2)
N(2)-Fe(1)-Cl(1)	92.60(5)	113.0(2)
N(3)-Fe(1)-Cl(1)	96.92(5)	103.1(3)
Cl(2)-Fe(1)-Cl(1)	114.84(2)	111.51(13)

The microanalytical data for all five complexes were consistent with compositions based on the general formula $LFeCl_2$. In addition, their IR spectra revealed ν(C=N) imine-stretching frequencies at around 1600 cm^{-1}, wavenumbers that are typical for that seen in similar *N*,*N*,*N*-iron complexes [3–8,19–24,31–34].

3.2. Ethylene Polymerization

In previous studies, precatalysts **A**–**E** (Scheme 1) exhibited their optimum performance for ethylene polymerization when activated with either modified methylaluminoxane (MMAO) or methylaluminoxane (MAO) [31–33,35]. Hence, this work is concerned with using both of these co-catalysts with **Fe2** chosen as the test precatalyst to permit an optimization of the reaction parameters. Changes to the run temperature, Al:Fe molar ratio, run time, and pressure will be independently undertaken for both **Fe2**/MMAO and **Fe2**/MAO before extending the corresponding set of optimized conditions to the remaining precatalysts, **Fe1**, **Fe3**, **Fe4**, and **Fe5** [19–24,28,31–34]. Typically, the polymerization runs will be performed in toluene at an ethylene pressure of 10 bar over a 30 min run time; the full set of data are collected in Tables 3 and 4. In all cases, differential scanning calorimetry (DSC) and gel permeation chromatography (GPC) are used to measure various polymer properties (M_w, M_w/M_n and T_m), while high-temperature NMR spectroscopy is employed for selected samples. As a matter of course, gas chromatography (GC) will be employed to check for any oligomeric products present in the polymerization solutions.

3.2.1. Catalytic Evaluation Using **Fe1**–**Fe5**/MMAO

In order to determine the optimal run temperature, **Fe2**/MMAO was screened at temperatures between 50 and 90 °C with the Al:Fe molar ratio fixed at 2000:1 (entries 1–5, Table 3). The highest activity of 11.2×10^6 g PE mol^{-1} (Fe) h^{-1} was observed at 70 °C. In terms of the molecular weight, all the polyethylenes displayed values between 7.0 and 12.2 kg mol^{-1} with temperature proving an influential factor. For example, the molecular weight of the polyethylene initially increased as the temperature of the run was raised from 50 to 70 °C and then decreased with a further rise in the reaction temperature; similar behavior has been reported for the *ortho*-cycloalkyl-containing **E** [22] (Scheme 1). It would seem the *ortho*-cyclohexyl groups in **Fe2** can protect the active iron species at temperatures up to 70 °C before the rate of chain transfer over chain propagation becomes more important at higher temperature. Across the temperature range explored, all the polyethylenes exhibited narrow unimodal distributions (M_w/M_n range = 2.3–3.1) indicative of single-site active species.

Table 3. Catalytic evaluation of **Fe1**–**Fe5** using modified methylaluminoxane (MMAO) as co-catalyst [a].

Entry	Precat.	Al:Fe	T/°C	t/min	Activity [b]	M_w [c]	M_w/M_n [c]	T_m [d]/°C
1	**Fe2**	2000	50	30	4.2	7.0	2.7	127.4
2	**Fe2**	2000	60	30	7.9	9.4	3.0	128.6
3	**Fe2**	2000	70	30	11.2	12.2	3.1	130.3
4	**Fe2**	2000	80	30	8.8	7.2	2.3	127.5
5	**Fe2**	2000	90	30	7.5	9.3	2.3	126.4
6	**Fe2**	1000	70	30	7.4	31.1	4.5	132.6
7	**Fe2**	1500	70	30	9.4	21.8	3.7	131.9
8	**Fe2**	2500	70	30	9.0	12.5	3.0	130.1
9	**Fe2**	3000	70	30	7.8	9.4	2.8	128.4
10	**Fe2**	2000	70	5	23.8	10.9	2.6	129.3
11	**Fe2**	2000	70	15	15.3	14.5	3.3	129.9
12	**Fe2**	2000	70	45	9.9	41.9	4.7	132.2
13	**Fe2**	2000	70	60	9.0	64.8	4.0	132.5
14 [e]	**Fe2**	2000	70	30	6.4	9.2	2.8	127.9
15	**Fe1**	2000	70	30	15.3	27.2	4.2	130.4
16	**Fe3**	2000	70	30	6.4	14.1	2.9	129.7
17	**Fe4**	2000	70	30	0.5	4.6	2.8	125.7
18	**Fe5**	2000	70	30	14.6	37.5	4.0	128.7

[a] Conditions: iron precatalyst (2.0 μmol), ethylene pressure (10 atm), toluene (100 mL). [b] Activity: 10^6 g PE per mol Fe per h. [c] M_w in kg per mol. M_w and M_w/M_n measured by gel permeation chromatography (GPC). [d] Measured using differential scanning calorimeter (DSC). [e] ethylene pressure (5 atm).

Then, the influence of the Al:Fe molar ratio was investigated using **Fe2**/MMAO (entries 3, 6–9, Table 3). Specifically, this ratio was increased from 1000:1 to 3000:1, resulting in a peak in activity being noted with 2000 molar equivalents of co-catalyst. Interestingly, all these runs maintained good activities (>7.4 × 10^6 g PE mol^{-1} (Fe) h^{-1}) even with lesser amounts of MMAO. With respect to the molecular weight of the polymer, this reached a maximum of 31.1 kg mol^{-1} when the Al:Fe molar ratio was 1000:1. As the ratio was raised, the molecular weight of the polyethylene decreased (Figure 3), which indicated that the rate of chain transfer increased; although uncertain at this stage, a process involving transfer of the polymer chain from the active iron catalyst to an alkyl-aluminum species seems likely [20,31,33,34,36,37].

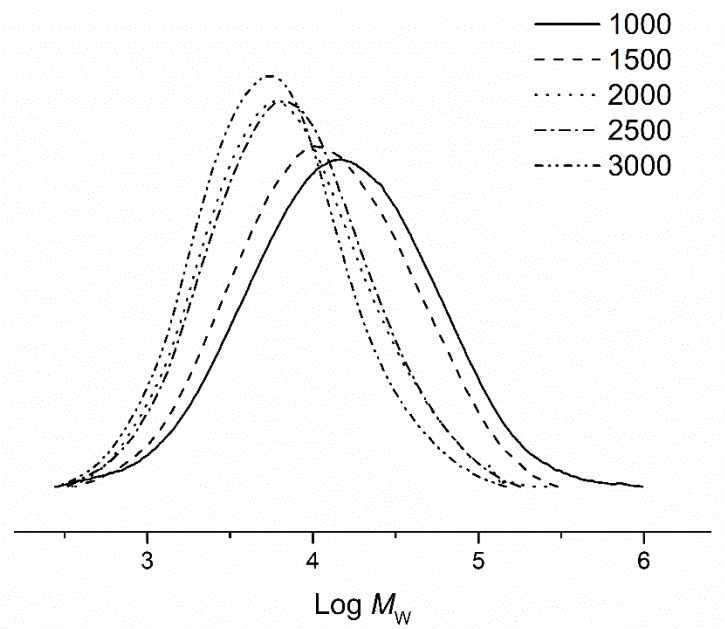

Figure 3. GPC traces of the polyethylene obtained using **Fe2**/MMAO at different Al:Fe molar ratios (entries 3, 6–9, Table 3).

With regard to the activity/time profile, the polymerization runs using **Fe2**/MMAO were quenched after pre-determined run times, typically 5, 15, 30, 45, and 60 min (entries 3 and 10–13, Table 3); the run temperature was kept at 70 °C and the molar ratio of Al to Fe was kept at 2000:1. An uppermost activity of 23.8×10^6 g PE mol^{-1} (Fe) h^{-1} was seen after 5 min (entries 10, Table 3) before a gradual decrease in catalytic activity was seen on extending the reaction time. Nonetheless, even after 60 min, the catalyst still maintained a credible activity (9.0×10^6 g PE mol^{-1} (Fe) h^{-1}), highlighting the sizable lifetime of this catalyst. On lowering the ethylene pressure from 10 to 5 atm (entries 3 and 14, Table 3), the catalytic activity showed a dramatic drop, while the polyethylene generated at the two different pressures possessed similar molecular weights and molecular weight distributions, which is a finding that is consistent with related iron analogs [22].

Based on the optimal polymerization conditions established for **Fe2**/MMAO, the remaining precatalysts **Fe1** and **Fe3**–**Fe5** were then investigated using MMAO as co-catalyst at 70 °C. A wide range in activities were observed between 0.5×10^6 g PE mol^{-1} (Fe) h^{-1} and 15.3×10^6 g PE mol^{-1} (Fe) h^{-1} (entries 3 and 15–18, Table 3). In terms of their relative performance, their activities were found to fall in the order: **Fe1**$_{C5H9/CHPh2}$~**Fe5**$_{C5H9/C5H9}$ > **Fe2**$_{C6H11/CHPh2}$ > **Fe3**$_{C8H15/CHPh2}$ > **Fe4**$_{C12H23/CHPh2}$ (Figure 4). Two key points emerge from the inspection of this order. Firstly, the cyclopentyl-containing precatalysts, **Fe1** and **Fe5**, displayed the highest activities with the benzhydryl-containing **Fe1** marginally higher. Secondly, the *ortho*-cycloalkyl ring size is of crucial importance to catalytic activity with the value observed using **Fe1** far exceeding that seen using **Fe2**, **Fe3**, and **Fe4**. Furthermore, **Fe1** gave the highest molecular weight polyethylene (27.2 kg mol^{-1}) of this series, which suggests that the cyclopentyl systems were more conducive to chain propagation and to the suppression of chain transfer. As for the dispersities of the polyethylene, **Fe1**–**Fe5**/MMAO all generated materials with M_w/M_n values that fell in the range 2.8–4.2, which is unlike the broad ranges often observed with structurally related iron analogs [19]. It would seem this class of catalyst has a predilection toward single site-like behavior.

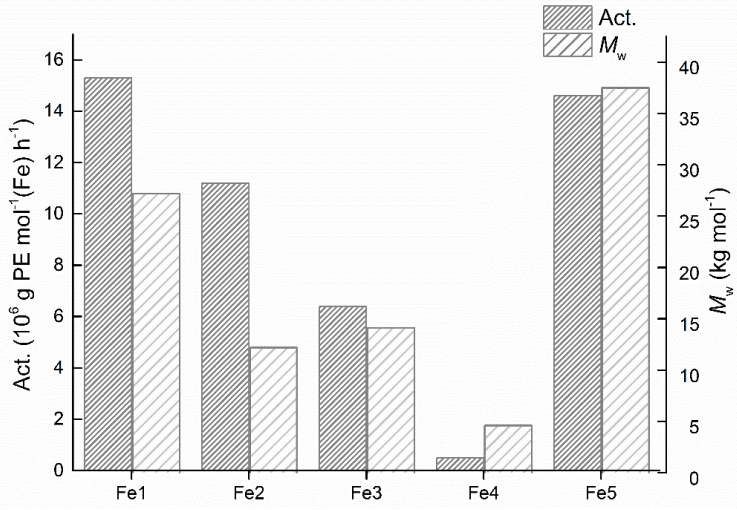

Figure 4. Variations in catalytic activity and molecular weight of the polyethylene obtained using **Fe1**–**Fe5** (entries 3, 15–18, Table 3); MMAO used as the co-catalyst in each case.

3.2.2. Catalytic Evaluation Using **Fe1**–**Fe5**/MAO

To allow a comparison with the MMAO study, we also studied the impact of using methylaluminoxane (MAO) as the activator for all five iron precatalysts. Complex **Fe2** was once again employed as the test precatalyst to optimize the conditions; the results of the evaluation are tabulated in Table 4. By maintaining the Al:Fe molar ratio at 2000:1, the highest activity of 3.3×10^6 g PE mol^{-1} (Fe) h^{-1} was achieved at 60 °C when investigated over the 30 to 80 °C temperature range (cf. 70 °C with **Fe2**/MMAO) (entry 4, Table 4). Although this level of performance was lower than that displayed using **Fe2**/MMAO (11.2×10^6 g PE mol^{-1} (Fe) h^{-1}), the molecular weight of the polyethylene reached

103.5 kg mol^{-1}, which is more than eight times that seen with MMAO. It is unclear as to the reason behind this molecular weight enhancement but it could plausibly be due to the greater stability of the active catalyst toward propagation over chain transfer at this lower temperature. Indeed, when the run temperature was raised to 70 °C, not only did the activity drop, but the molecular weight of the polymer significantly declined as well (entry 5, Table 4 and Figure 5).

Table 4. Catalytic evaluation of **Fe1**–**Fe5** using MAO as co-catalyst [a].

Entry	Precat	Al:Fe	T/°C	t/min	Activity [b]	M_w [c]	M_w/M_n [c]	T_m [d]/°C
1	**Fe2**	2000	30	30	2.7	45.8	2.7	135.0
2	**Fe2**	2000	40	30	2.9	90.6	3.0	132.6
3	**Fe2**	2000	50	30	3.1	32.0	3.1	134.6
4	**Fe2**	2000	60	30	3.3	103.5	2.3	131.9
5	**Fe2**	2000	70	30	1.2	25.9	2.3	133.8
6	**Fe2**	2000	80	30	1.0	24.7	4.5	131.1
7	**Fe2**	1000	60	30	1.0	186.8	3.7	135.1
8	**Fe2**	1500	60	30	2.9	41.6	3.0	132.2
9	**Fe2**	2500	60	30	4.1	35.5	2.8	131.7
10	**Fe2**	3000	60	30	2.7	13.6	2.6	130.3
11	**Fe2**	2500	60	5	7.2	88.9	3.3	133.1
12	**Fe2**	2500	60	15	5.6	52.8	4.7	132.3
13	**Fe2**	2500	60	45	2.9	44.5	4.0	132.5
14	**Fe2**	2500	60	60	2.4	71.2	2.8	134.2
15 [e]	**Fe2**	2500	60	30	1.2	28.8	3.2	133.0
16	**Fe1**	2500	60	30	5.3	55.6	2.9	131.8
17	**Fe3**	2500	60	30	1.6	11.2	2.8	131.3
18	**Fe4**	2500	60	30	0.3	5.1	4.0	129.6
19	**Fe5**	2500	60	30	6.0	25.6	2.7	131.0

[a] Conditions: iron precatalyst (2.0 μmol), ethylene pressure (10 atm), toluene (100 mL). [b] Activity: 10^6 g PE per mol Fe per h. [c] M_w in kg per mol. M_w and M_w/M_n measured by GPC. [d] Measured by DSC. [e] ethylene pressure (5 atm).

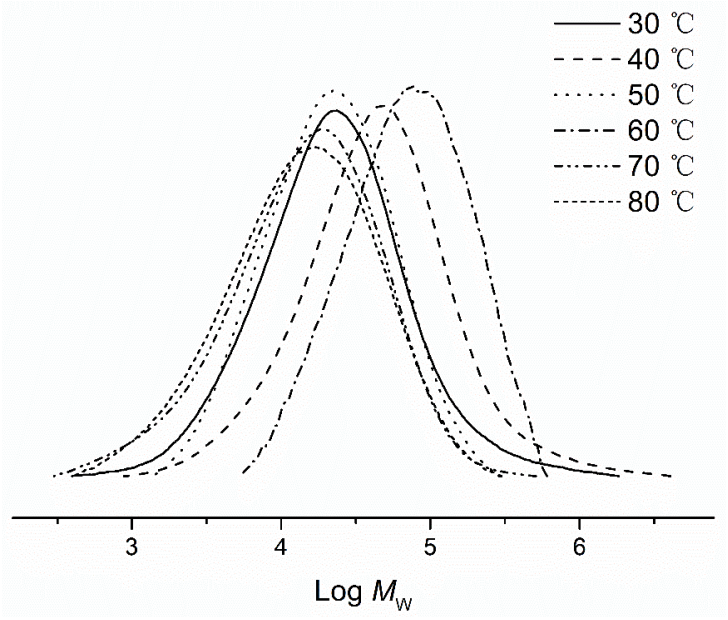

Figure 5. GPC traces of the polyethylene obtained using **Fe2**/MAO at different temperatures (entries 1–6, Table 4).

With the reaction temperature maintained at 60 °C, a series of polymerization runs were conducted using **Fe2**/MAO with the Al:Fe molar ratio systematically raised from 1000:1 to 3000:1 (entries 4 and 7–10, Table 4). A peak activity of 4.1 × 10^6 g PE mol^{-1} (Fe) h^{-1} was observed with an Al:Fe molar ratio

of 2500:1 (entry 9, Table 4). On increasing the molar ratio above 2500:1, a decline in activity was seen which is consistent with more chain transfer (Figure 6) [19,22,33,38].

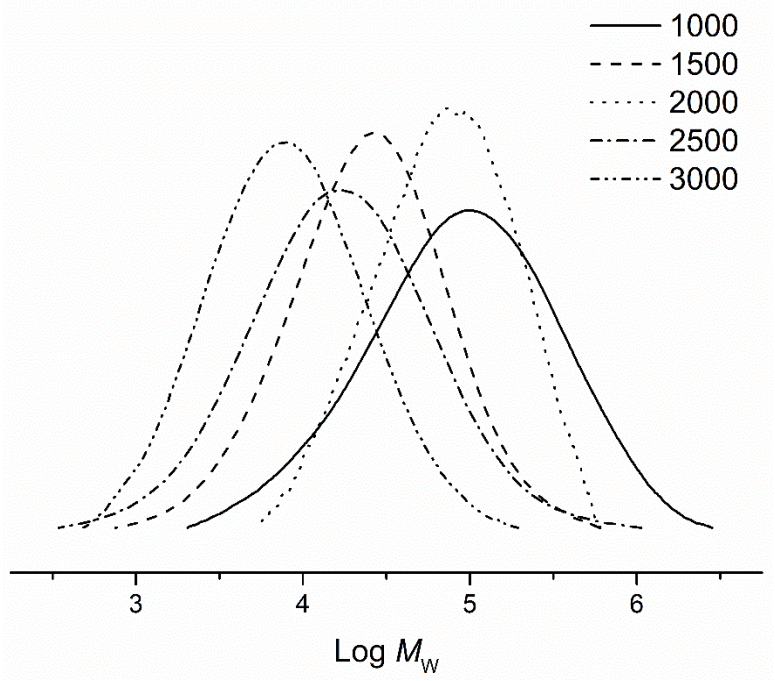

Figure 6. GPC traces of the polyethylene obtained using **Fe2**/MAO at different Al:Fe molar ratios (entries 4 and 7–10, Table 4).

As with **Fe2**/MMAO, the activity dropped as the run time was extended though not as noticeably (entries 9 and 11–14, Table 4). Hence, at the five minute mark, a value of 7.2×10^6 g of PE mol^{-1} (Fe) h^{-1} was achieved that only decreased to 2.4×10^6 g of PE mol^{-1} (Fe) h^{-1} after 60 min (entry 11, Table 4, and entry 14, Table 4). It is apparent that this catalyst though less active than **Fe2**/MMAO maintained a more uniform activity/time profile. As with **Fe2**/MMAO, a short induction period is needed to reach peak performance with **Fe2**/MAO; similar observations have been noted elsewhere for iron and cobalt catalysts [39].

With the optimal polymerization conditions identified for **Fe2**/MAO (*viz.*, an Al:Fe molar ratio = 2500:1, run temperature = 60 °C, run time = 30 min), the four other iron precatalysts, **Fe1** and **Fe3**–**Fe5**, were also evaluated using these set of conditions; their results are displayed alongside **Fe2** in Table 4 (entries 9 and 16–19). Examination of the data reveals that these iron precatalysts exhibited a range in activities from 0.3 to 6.0×10^6 g of PE mol^{-1} (Fe) h^{-1} which is narrower than that seen with MMAO. In terms of their relative performance, their catalytic activities fell in the order: **Fe5**$_{C5H9/C5H9}$~**Fe1**$_{C5H9/CHPh2}$ > **Fe2**$_{C6H11/CHPh2}$ > **Fe3**$_{C8H15/CHPh2}$ > **Fe4**$_{C12H23/CHPh2}$. This order essentially mirrors that seen with MMAO, although closer inspection reveals **Fe1** to be slightly more active than **Fe5** (the opposite was seen with MMAO). Once again, the catalytic activity is shown to drop as the size of the *ortho*-cycloalkyl ring was increased from 5 to 12 (Figure 7). One possible explanation for this observation may relate to steric protection imparted by the larger cycloalkyl rings on the active iron center, thereby impeding ethylene coordination and insertion. In addition, the molecular weight of the polyethylene was found to drop from 55.6 to 5.1 kg mol^{-1} as the *ortho*-cycloalkyl increased, reaching the minimum value for the most sterically hindered **Fe4** (Figure 7). Nonetheless, the dispersities remained narrow for all five catalysts (M_w/M_n range: 2.7–4.0).

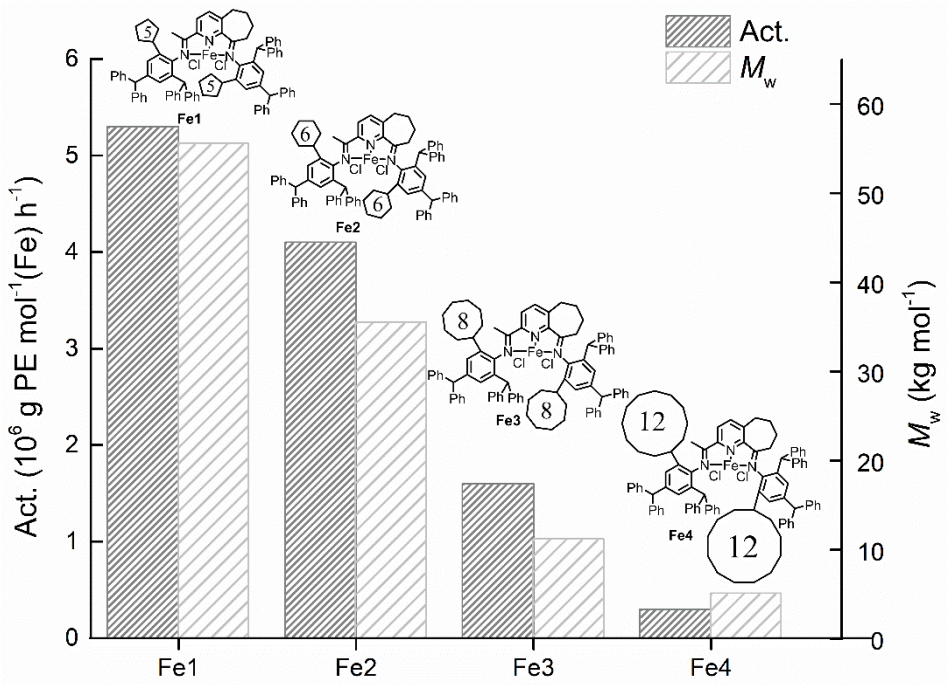

Figure 7. Variations in catalytic activity and molecular weight of the polyethylene displayed using **Fe1**–**Fe4** (entries 9, 16–18, Table 4); MAO used as the co-catalyst in each case.

3.3. Microstructural Properties of the Polyethylene

As highlighted in Tables 3 and 4, the melting points displayed by the polyethylenes fell between 126.4 and 135.1 °C, which is characteristic of linear polyethylene [32,35,37]. To confirm this assertion and gather more information about the end group composition and likely chain transfer pathways, samples of polyethylene obtained using **Fe2**/MAO and **Fe2**/MMAO have been analyzed by ^{1}H and ^{13}C NMR spectroscopy (recorded in tetrachloroethane-d_2 at 100 °C).

As shown in Figure 8, the ^{1}H NMR spectrum of the polymer generated using **Fe2**/MMAO (M_w = 12.2 kg mol^{-1}; entry 3, Table 3) revealed resonances typical of a –C(H$_b$)=C(H$_a$)$_2$ end group, which was backed up by the ^{13}C NMR spectrum with the corresponding vinylic carbon signals visible at δ 116.5 and 139.0 [19,40–42]. Such an observation would imply that β-hydrogen elimination is a major chain transfer pathway. However, on inspection of the ratio of the integrals for the vinylic H$_a$ to methyl H$_g$ protons (δ 0.97) in the ^{1}H NMR spectrum, a slight excess of the expected 2:3 ratio was evident, signifying the co-existence of some fully saturated polyethylene. This finding would suggest that a termination mechanism involving chain transfer to AlMe$_3$ (but not Al(*i*-Bu$_3$)), and its aluminum derivatives found in MMAO solutions, also plays a minor role [20,22]. In addition, carbon signals corresponding to saturated *n*-butyl end chain ends were clearly visible in the lower frequency region of the ^{13}C NMR spectrum (d, e, f and g, Figure 8).

In addition, a sample of the higher molecular weight (M_w = 35.3 kg mol^{-1}) polyethylene prepared using **Fe2**/MAO at 60 °C (entry 9, Table 4) was characterized by ^{13}C NMR spectroscopy. High-intensity singles observed around δ 29.44 (see Figure 9) were the only signals detectable which can be assigned to the –(CH$_2$)$_n$– repeat unit in accord with high linearity of the material. No clear evidence was found to support the existence of unsaturated nor saturated chain ends presumably due to the high molecular weight of this sample.

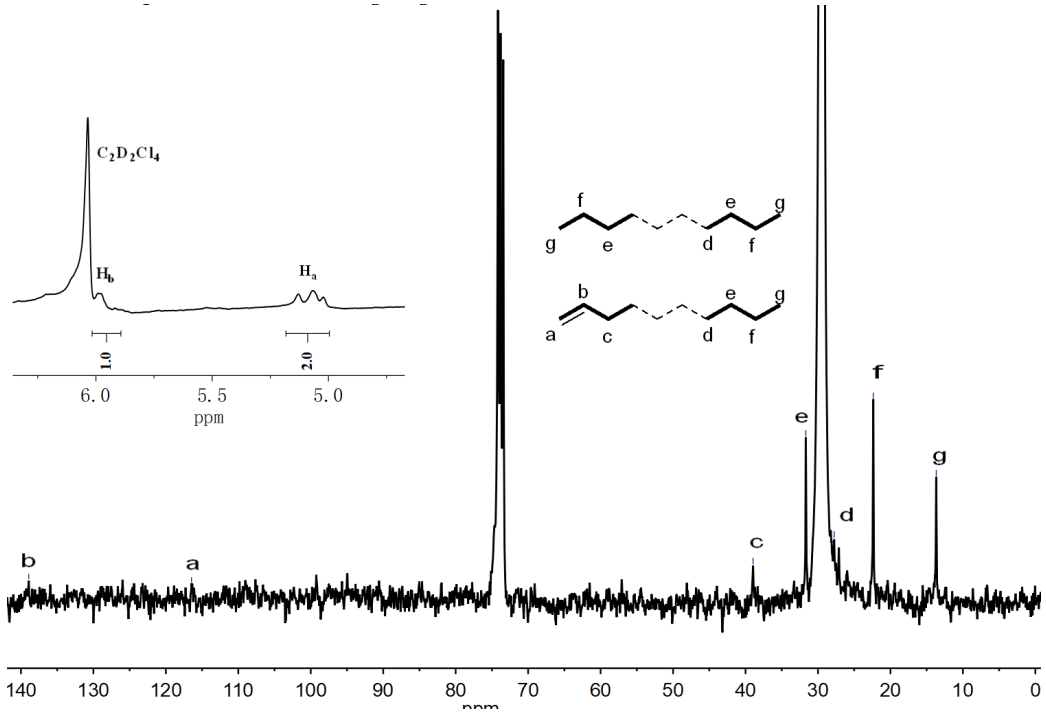

Figure 8. ^{13}C NMR spectrum of the polyethylene obtained using **Fe2**/MMAO (entry 3, Table 3) along with an insert showing the vinylic region of its ^{1}H NMR spectrum (**a**–**g**); both spectra recorded in tetrachloroethane-d_2 at 100 °C.

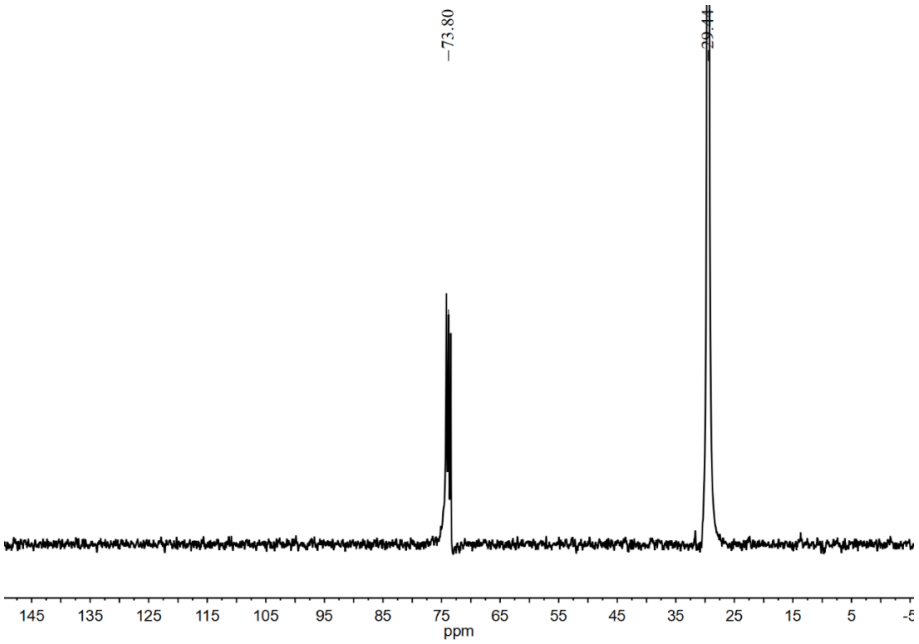

Figure 9. ^{13}C NMR spectrum of the polyethylene generated using **Fe2**/MAO at 60 °C (entry 9, Table 4); recorded in tetrachloroethane-d_2 at 100 °C (δC 73.8).

4. Conclusions

The bis(arylimino)tetrahydrocyclohepta[*b*]pyridine dichloroiron(II) complexes, **Fe1**–**Fe4**, comprising *N*-aryl groups appended with benzhydryl/cycloalkyl *ortho*-substituents have been successfully synthesized; in addition, **Fe5** based on a cyclopentyl/cyclopentyl *ortho*-pairing is also disclosed. All five complexes have been fully characterized including by single crystal X-ray diffraction

in the cases of **Fe3** and **Fe5**. On their treatment of **Fe1**–**Fe5** with either MAO or MMAO, a range in catalytic activities was exhibited with cyclopentyl-containing **Fe1** and **Fe5** at the top end for both activators. Indeed, **Fe1**/MMAO achieved exceptionally high activity at a temperature of 70 °C (1.53×10^7 g PE per mol Fe per h) underlining the appreciable thermostability of this iron catalytic system. Furthermore, the activities were found to drop as the *ortho*-cycloalkyl ring size increased with the most sterically encumbered cyclododecyl-containing **Fe4** displaying only modest activity. In a similar fashion, the molecular weights for the polymers were also found to decline as the ring size increased with cyclopentyl-containing **Fe1**/MAO producing the highest molecular weight polyethylene of the MAO-activated series (55.6 kg mol^{-1}). Strictly linear polyethylene (T_m > 126 °C) with narrow distribution (M_w/M_n range: 2.3–4.7) were features of all the polymers generated in this study, the latter highlighting the good control of these polymerizations. Despite the high molecular weights, end group analysis revealed evidence for vinyl-terminated polymers supporting the role of β-hydride elimination as a key chain transfer pathway.

Supplementary Materials: The following are available online at http://www.mdpi.com/2073-4344/10/9/1002/s1, X-ray crystallographic data for **Fe3** and **Fe5**. CCDC: 2021622 (**Fe3**), 2020110 (**Fe5**).

Author Contributions: Design of the study by G.A.S. and W.-H.S., design of the anilines by I.I.O.; synthesis of the organic compounds by M.H., I.I.O. and I.V.O.; synthesis of the iron complexes by M.H. and Q.Z.; characterization by M.H., I.I.O., I.V.O., Y.M. and W.-H.S.; X-ray study by. T.L. and G.A.S.; catalytic study by M.H. and H.S.; characterization of the polyethylenes by M.H., H.S. and Y.M.; writing, editing, and polishing by M.H., G.A.S., I.I.O. and W.-H.S. All authors have read and agreed to the published version of the manuscript.

Funding: This work was funded by the National Natural Science Foundation of China (No. 21871275).

Acknowledgments: GAS is grateful to the Chinese Academy of Sciences for a President's International Fellowship for Visiting Scientists.

Conflicts of Interest: The authors declare no conflict of interest.

References

1. Natta, G.; Pino, P.; Corradini, P.; Danusso, F.; Mantica, E.; Mazzanti, G.; Moraglio, G. Crystalline high polymers of α-olefins. *J. Am. Chem. Soc.* **1955**, *77*, 1708–1710. [CrossRef]
2. Stürzel, M.; Mihan, S.; Mülhaupt, R. From Multisite Polymerization Catalysis to Sustainable Materials and All-Polyolefin Composites. *Chem. Rev.* **2016**, *116*, 1398–1433. [CrossRef] [PubMed]
3. Flisak, Z.; Sun, W.-H. Progression of Diiminopyridines: From Single Application to Catalytic Versatility. *ACS Catal.* **2015**, *5*, 4713–4724. [CrossRef]
4. Wang, Z.; Solan, G.A.; Zhang, W.; Sun, W.-H. Carbocyclic-fused N,N,N-pincer ligands as ring-strain adjustable supports for iron and cobalt catalysts in ethylene oligo-/polymerization. Coord. *Chem. Rev.* **2018**, *363*, 92–108. [CrossRef]
5. Burcher, B.; Breuil, P.-A.R.; Magna, L.; Olivier-Bourbigou, H. Iron-Catalyzed Oligomerization and Polymerization Reactions. *Top. Organomet. Chem.* **2015**, *50*, 217–258.
6. Britovsek, G.J.P.; Mastroianni, S.; Solan, G.A.; Baugh, S.P.D.; Redshaw, C.; Gibson, V.C.; White, A.J.P.; Williams, D.J.; Elsegood, M.R.J. Oligomerisation of Ethylene by Bis(imino)pyridyliron and -cobalt Complexes. *Chem. Eur. J.* **2000**, *6*, 2221–2231. [CrossRef]
7. Britovsek, G.J.P.; Gibson, V.C.; Hoarau, O.D.; Spitzmesser, S.K.; White, A.J.P.; Williams, D.J. Iron and Cobalt Ethylene Polymerization Catalysts: Variations on the Central Donor. *Inorg. Chem.* **2003**, *42*, 3454–3465. [CrossRef]
8. Zhang, Q.; Wu, N.; Xiang, J.; Solan, G.A.; Suo, H.; Ma, Y.; Liang, T.; Sun, W.-H. Bis-cycloheptyl-fused bis(imino)pyridine-cobalt catalysts for PE wax formation: Positive effects of fluoride substitution on catalytic performance and thermal stability. *Dalton Trans.* **2020**, *49*, 9425–9437. [CrossRef]
9. Small, B.L.; Brookhart, M. Highly Active Iron and cobalt Catalysts for the Polymerization of Olefins. *J. Am. Chem. Soc.* **1998**, *120*, 4049–4050. [CrossRef]
10. Britovsek, G.J.P.; Gibson, V.C.; Kimberley, B.S.; Maddox, P.J.; McTavish, S.J.; Solan, G.A.; White, A.J.P.; Williams, D.J. Novel olefin polymerization catalysts based on iron and cobalt. *Chem. Commun.* **1998**, *7*, 849–850. [CrossRef]

11. Britovsek, G.J.P.; Bruce, M.; Gibson, V.C.; Kimberley, B.S.; Maddox, P.J.; Mastroianni, S.; McTavish, S.J.; Redshaw, C.; Solan, G.A.; Strömberg, S.; et al. Iron and cobalt Ethylene Polymerization Catalysts Bearing 2,6-Bis(Imino)Pyridyl Ligands: Synthesis, Structures, and Polymerization Studies. *J. Am. Chem. Soc.* **1999**, *121*, 8728–8740. [CrossRef]
12. Small, B.L. Discovery and Development of Pyridine-bis(imine) and Related Catalysts for Olefin Polymerization and Oligomerization. *Acc. Chem. Res.* **2015**, *48*, 2599–2611. [CrossRef] [PubMed]
13. Small, B.L.; Brookhart, M. Iron-Based Catalysts with Exceptionally High Activities and Selectivities for Oligomerization of Ethylene to Linear r-Olefins. *J. Am. Chem. Soc.* **1998**, *120*, 7143–7144. [CrossRef]
14. Wang, Z.; Liu, Q.; Solan, G.A.; Sun, W.-H. Recent advances in Ni-mediated ethylene chain growth: Nimine-donor ligand effects on catalytic activity, thermal stability and oligo-/polymer structure. *Coord. Chem. Rev.* **2017**, *350*, 68–83. [CrossRef]
15. Yuan, S.; Fan, Z.; Zhang, Q.; Flisak, Z.; Ma, Y.; Sun, W.-H. Enhancing performance of α-diiminonickel precatalyst for ethylene polymerization by substitution with the 2,4-bis(4,4′-dimethoxybenzhydryl)-6-methylphenyl group. *Appl. Organomet. Chem.* **2020**, *34*, e5638. [CrossRef]
16. Bariashir, C.; Huang, C.; Solan, G.A.; Sun, W.-H. Recent advances in homogeneous chromium catalyst design for ethylene tri-, tetra-, oligo and polymerization. *Coord. Chem. Rev.* **2019**, *385*, 208–229. [CrossRef]
17. Gansukh, B.; Zhang, Q.; Flisak, Z.; Liang, T.; Ma, Y.; Sun, W.-H. The chloro-substituent enhances performance of 2,4-bis(imino)pyridylchromium catalysts yielding highly linear polyethylene. *Appl. Organomet. Chem.* **2020**, *34*, e5471. [CrossRef]
18. Phillips, A.; Suo, H.; Silva, M.; Pombeiro, A.; Sun, W.-H. Recent developments in vanadium-catalyzed olefin coordination polymerization. *Coord. Chem. Rev.* **2020**, *416*, e213332. [CrossRef]
19. Du, S.; Wang, X.; Zhang, W.; Flisak, Z.; Sun, Y.; Sun, W.-H. A practical ethylene polymerization for vinyl-polyethylenes: Synthesis, characterization and catalytic behavior of α,α′-bisimino-2,3:5,6-bis(pentamethylene)pyridyliron chlorides. *Polym. Chem.* **2016**, *7*, 4188–4197. [CrossRef]
20. Bariashir, C.; Wang, Z.; Ma, Y.; Vignesh, A.; Hao, X.; Sun, W.-H. Finely Tuned α,α′-Bis(arylimino)-2,3:5,6-bis(pentamethylene)pyridine-Based Practical Iron Precatalysts for Targeting Highly Linear and Narrow Dispersive Polyethylene Waxes with Vinyl Ends. *Organometallics* **2019**, *38*, 4455–4470. [CrossRef]
21. Huang, F.; Xing, Q.; Liang, T.; Flisak, Z.; Ye, B.; Hu, X.; Yang, W.; Sun, W.-H. 2-(1-Aryliminoethyl)-9-arylimino-5,6,7,8-tetrahydrocycloheptapyridyl iron(II) dichloride: Synthesis, characterization, and the highly active and tunable active species in ethylene polymerization. *Dalton Trans.* **2014**, *43*, 16818–16829. [CrossRef] [PubMed]
22. Guo, J.; Zhang, W.; Oleynik, I.I.; Solan, G.A.; Oleynik, I.V.; Liang, T.; Sun, W.-H. Probing the effect of ortho-cycloalkyl ring size on activity and thermostability in cycloheptyl-fused N,N,N-iron ethylene polymerization catalysts. *Dalton Trans.* **2020**, *49*, 136–146. [CrossRef] [PubMed]
23. Suo, H.; Li, Z.; Oleynik, I.V.; Wang, Z.; Oleynik, I.I.; Ma, Y.; Liu, Q.; Sun, W.-H. Achieving strictly linear polyethylenes by the NNN-Fe precatalysts finely tuned with different sizes of ortho-cycloalkyl substituents. *Appl. Organomet. Chem.* **2020**, e5937. [CrossRef]
24. Wang, Z.; Solan, G.A.; Ma, Y.; Liu, Q.; Liang, T.; Sun, W.-H. Fusing carbocycles of inequivalent ring size to a bis(imino)pyridine-iron ethylene polymerization catalyst; distinctive effects on activity, PE molecular weight and dispersity. *Research* **2019**, *2019*, e9426063. [CrossRef] [PubMed]
25. Xie, X.; Huang, H.; Mo, W.; Fan, X.; Shen, Z.; Sun, N.; Hu, B.; Hu, X. Tetrahedron: Asymmetry. *Sci. Direct* **2009**, *20*, 1425–1432.
26. Oleinik, I.I.; Oleinik, I.V.; Abdrakhmanov, I.B.; Ivanchev, S.S.; Tolstikov, G.A. Design of Arylimine Postmetallocene Catalytic Systems for Olefin Polymerization: I. Synthesis of Substituted 2-Cycloalkyl and 2,6-Dicycloalkylanilines. *Russ. J. Gen. Chem.* **2004**, *74*, 1423–1427. [CrossRef]
27. Chartoire, A.; Claver, C.; Corpet, M.; Krinsky, J.; Mayen, J.; Nelson, D.; Nolan, S.P.; Penafiel, I.; Woodward, R.; Meadows, R.E. Recycle NHC Catalyst for the Development of a Generalized Approach to Continuous Buchwald-Hartwing Reaction and Workup. *Org. Process Res. Dev.* **2016**, *20*, 551–557. [CrossRef]
28. Han, M.; Zhang, Q.; Oleinik, I.I.; Suo, H.; Solan, G.A.; Oleinik, I.V.; Ma, Y.; Liang, T.; Sun, W.-H. High molecular weight polyethylenes of narrow dispersity promoted using bis(arylimino)cyclohepta[b]pyridine-cobalt catalysts ortho-substituted with benzhydryl & cycloalkyl groups. *Dalton Trans.* **2020**, *49*, 4774–4784.
29. Sheldrick, G.M. SHELXT: Integrated space-group and crystalstructure determination. *Acta Crystallogr. Sect. A* **2015**, *71*, 3–8. [CrossRef]

30. Sheldrick, G.M. Crystal structure refinement with SHELXL. *Acta Crystallogr. Sect. C* **2015**, *71*, 3–8. [CrossRef]
31. Guo, J.J.; Wang, Z.; Zhang, W.; Oleynik, I.I.; Vignesh, A.; Oleynik, I.V.; Hu, X.; Sun, Y.; Sun, W.-H. Highly Linear Polyethylenes Achieved Using Thermo-Stable and Efficient Cobalt Precatalysts Bearing Carbocyclic-Fused NNN-Pincer Ligand. *Molecules* **2019**, *24*, 1176. [CrossRef]
32. Zhang, R.; Ma, Y.; Han, M.; Solan, G.A.; Pi, Y.; Sun, Y.; Sun, W.-H. Exceptionally high molecular weight linear polyethylene by using N,N,N'-Co catalysts appended with a N'-2,6-bis{di(4-fluorophenyl)methyl} -4-nitrophenyl group. *Appl. Organomet. Chem.* **2019**, *33*, e5157. [CrossRef]
33. Zhang, Q.; Ma, Y.; Suo, H.; Solan, G.A.; Liang, T.; Sun, W.-H. Co-catalyst effects on the thermal stability/activity of N,N,N-Co ethylene polymerization Catalysts Bearing Fluoro-Substituted N-2,6-dibenzhydrylphenyl groups. *Appl. Organomet. Chem.* **2019**, *33*, e5134. [CrossRef]
34. Zada, M.; Guo, L.; Ma, Y.; Zhang, W.; Flisak, Z.; Sun, Y.; Sun, W.-H. Activity and Thermal Stability of Cobalt(II)-Based Olefin Polymerization Catalysts Adorned with Sterically Hindered Dibenzocycloheptyl Groups. *Molecules* **2019**, *24*, 2007. [CrossRef]
35. Huang, F.; Zhang, W.; Yue, E.; Liang, T.; Hu, X.; Sun, W.-H. Controlling the molecular weights of polyethylene waxes using the highly active precatalysts of 2-(1-aryliminoethyl)-9-arylimino-5,6,7,8-tetrahydrocycloheptapyridylCobalt chlorides: Synthesis, characterization, and catalytic behavior. *Dalton Trans.* **2016**, *45*, 657–666. [CrossRef]
36. Chen, Q.; Zhang, W.; Solan, G.A.; Liang, T.; Sun, W.-H. Methylene-bridged bimetallic bis(imino)pyridinecobaltous chlorides as precatalysts for vinyl-terminated polyethylene waxes. *Dalton Trans.* **2018**, *47*, 6124–6133. [CrossRef]
37. Suo, H.; Oleynik, I.I.; Bariashir, C.; Oleynik, I.V.; Wang, Z.; Solan, G.A.; Ma, Y.; Liang, T.; Sun, W.-H. Strictly linear polyethylene using Fe-catalysts chelated by fused bis(arylimino)pyridines: Probing ortho-cycloalkyl ring-size effects on molecular weight. *Polymer* **2018**, *149*, 45–54. [CrossRef]
38. Appukuttan, V.K.; Liu, Y.; Son, B.C.; Ha, C.-S.; Suh, H.; Kim, I.I. Iron and cobalt complexes of 2,3,7,8-tetrahydroacridine-4,-5(1H,6H)-diimine sterically modulated by substituted aryl rings for the selective oligomerization to polymerization of ethylene. *Organometallics* **2011**, *30*, 2285–2294. [CrossRef]
39. Xiao, T.; Hao, P.; Kehr, G.; Hao, X.; Erker, G.; Sun, W.-H. Dichlorocobalt(II) Complexes Ligated by Bidentate 8-(Benzoimidazol-2-yl)quinolines: Synthesis, Characterization, and Catalytic Behavior toward Ethylene. *Organometallics* **2011**, *30*, 4847–4853. [CrossRef]
40. Hansen, E.; Blom, R.; Bade, O. NMR characterization of polyethylene with emphasis on internal consistency of peak intensities and estimation of uncertainties in derived branch distribution numbers. *Polymer* **1997**, *38*, 4295–4304. [CrossRef]
41. Galland, G.; Quijada, R.; Rolas, R.; Bazan, G.; Komon, Z. NMR Study of Branched Polyethylenes Obtained with Combined Fe and Zr Catalysts. *Macromolecules* **2002**, *35*, 339–345. [CrossRef]
42. Semikolenova, N.; Sun, W.-H.; Soshnikov, I.; Matsko, M.; Kolesova, O.; Zakharov, V.; Bryliakov, K. Origin of "Multisite-like" Ethylene Polymerization Behavior of the Single-Site Nonsymmetrical Bis(imino)pyridine Iron(II) Complex in the Presence of Modified Methylaluminoxane. *ACS Catal.* **2017**, *7*, 2868–2877. [CrossRef]